

Effect of melt spinning conditions on the fiber structure development of polyethylene terephthalate

R. Tomisawa^a, T. Ikaga^a, K. H. Kim^a, Y. Ohkoshi^{a,b,*}, K. Okada^c,
H. Masunaga^d, T. Kanaya^e, M. Masuda^f, Y. Maeda^f

^a*Faculty of Textile Science and Technology, Shinshu University, 3-15-1 Tokida, Ueda, Nagano 386-8567, Japan.*

^b*Institute for Fiber Engineering, Shinshu University Tokida 3-15-1, Ueda, Nagano prefecture, 386-8567, Japan.*

^c*Material Science Laboratories, Toray Research Center, Inc, 3-3-7 Sonoyama, Otsu, Shiga 520-8567, Japan.*

^d*Japan Synchrotron Radiation Research Institute, 1-1-1 Kouto, Sayo-cho, Sayo-gun, Hyogo 679-5148, Japan.*

^e*High Energy Accelerator Research Organization, 203-1 Shirakata, Tokai-mura, Naka-gun, Ibaraki, 319-1106, Japan.*

^f*Toray Industries, Inc, 4845 Mishima, Shizuoka 411-8652, Japan.*

*Corresponding author. *E-mail address:* yokoshi@shinshu-u.ac.jp (Y. Okoshi)

Abstract

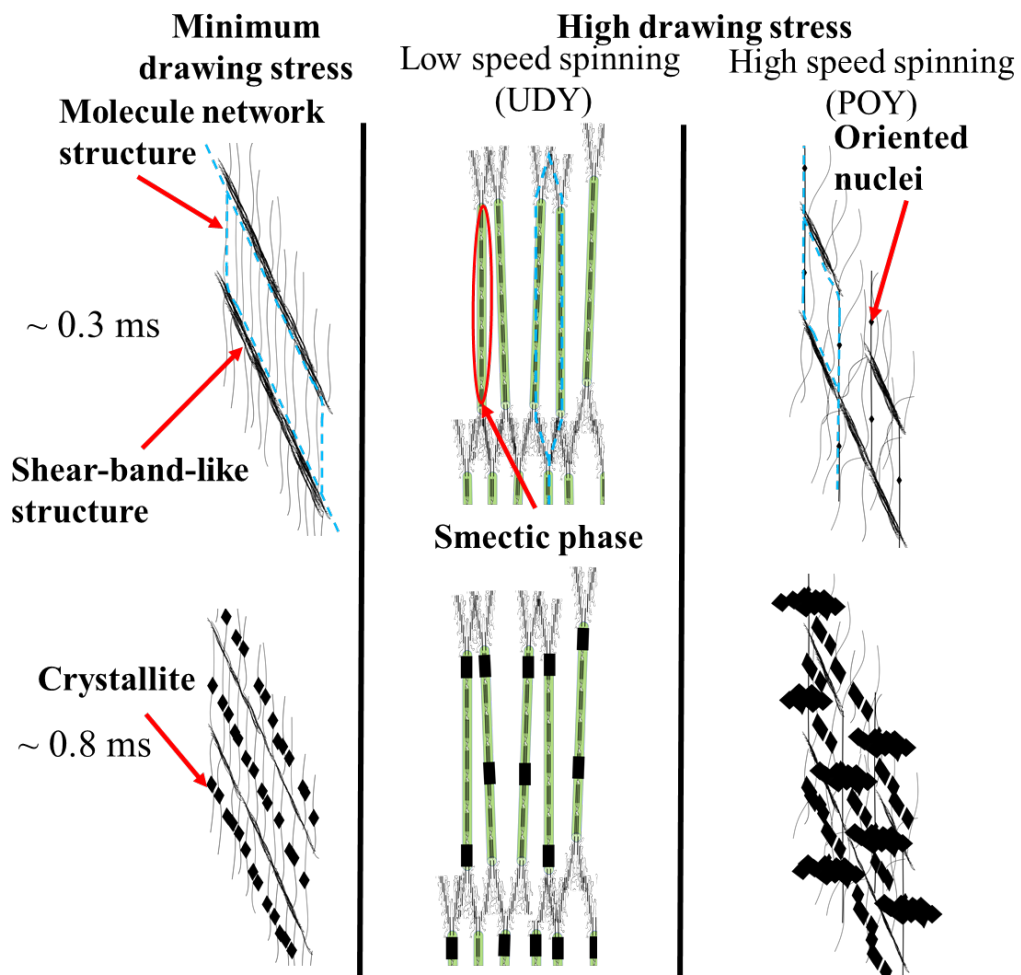
The effects of spinning conditions on fiber properties are not well explained by the fiber structures because the birefringence, crystallinity, and SAXS patterns are often similar. In this study, the effects on the fiber structure development of polyethylene terephthalate after necking was analyzed by simultaneous WAXD/SAXS measurements. An X-shaped SAXS pattern was observed for all fibers drawn at the minimum draw ratio. In contrast, by drawing under a drawing stress of 100 MPa, the strong diffraction of the smectic phase and an obviously larger long period less than 1 μm after necking were observed for fibers spun at 500–1500 m/min, while almost no smectic phase was observed for fibers spun at 2000 m/min. A higher crystallization rate and clear draw ratio dependence of crystallization rate were also observed for the fiber spun at 2000 m/min. The clear differences in structure development can explain their differences in tensile strength and thermal shrinkage.

Keywords: polyethylene terephthalate; X-ray diffraction; X-ray scattering; smectic phase; fiber; strength

Highlights

- Fiber structure development of PET fibers spun at 500–2000 m/min was analyzed.
- X-shaped SAXS patterns were observed for fibers drawn at the minimum stable ratio.
- Smectic phase was formed by the high-ratio drawing of fibers spun at low speed.
- SAXS patterns less than 1 ms after necking showed spinning condition dependence.
- Structure development differences reflect the property variations of drawn fibers.

Graphical abstract



1. Introduction

Polyethylene terephthalate (PET) fibers are widely used synthetic fibers. There are a multitude of studies on the structure and physical properties of PET fibers. The mechanical and thermomechanical properties of highly drawn fibers strongly depend on melt spinning conditions. However, the effect of melt spinning conditions on structural parameters such as birefringence, crystallinity, and crystal orientation factor is too small to explain the observed differences in the properties of PET fibers. In this study, we try to explain the effect of melt spinning conditions on the above-mentioned physical properties of resultant fibers focusing on the fiber structure development process.

The structure of a PET fiber is mostly determined by the drawing process. However, the properties of the obtained fiber are also influenced by the spinning conditions because they determine the maximum draw ratio. Indeed, the spinning conditions are selected to fit the application of the fibers being produced. For example, a partially oriented yarn (POY) is obtained at a spinning speed of 2000–4000 m/min under a high spin-line tension. POYs are suitable to produce fibers with a high modulus and low shrinkage, and are used in products requiring dimensional stability at high temperature, like tire cords. Meanwhile, high-tenacity fibers can be prepared by spinning at low speed and then drawing to a high draw ratio. High-tenacity fibers are used in products requiring high tensile strength, like seat belts [1]. In recent years, a new spinning procedure called laser spinning has been proposed [2, 3]. In this procedure, rapid fiber heating by a laser beam irradiated onto molten fibers lowers the spin-line stress with minimal thermal decomposition. The resulting fibers possess a uniform network structure, which leads to the improved tensile strength of the maximally drawn fibers [2]. There have been similar trials for producing high-strength fibers, collectively referred to as “melt structure control”, which formed uniform molecular network structures by controlling the melt spinning process [2-9].

Fiber structure development after neck drawing has been observed for PET [10-13, 18], polyethylene naphthalate (PEN) [14], polypropylene [15], polyphenylene sulfide [16], and polybutylene terephthalate (PBT) [17] in wide-angle X-ray diffraction (WAXD) and small-angle X-ray scattering (SAXS) images captured with synchrotron X-rays at SPring-8. In particular, we previously analyzed the effect of the draw ratio on the fiber structure development of PET [10]. We found that the amount of smectic phase increased with draw ratio until a certain point, and then the d-spacing of the smectic phase enlarged as draw ratio further increased. These results could explain the change of mechanical and thermomechanical properties of drawn fibers, which means the analysis of fiber structure development can be considered as a new valuable structure evaluation procedure to design the physical properties of drawn fibers. We use the same procedure to investigate the effects of spinning conditions on fiber structure development in this study. That is, here we analyze the effects of a spinning speed of 500–2000 m/min and laser spinning on the development of PET fiber structure. The fiber structure development is analyzed by measuring the time dependence of structural

parameters including the amount of smectic phase, d-spacing of smectic phase, degree of crystallinity, and long period.

2. Experimental

2.1. Samples

The fibers used for drawing in this study were prepared by melt spinning PET (IV=1.3 dL/g) provided by Toray Co. The polymer was heated 310 °C, extruded from a nozzle with a single hole at a mass flow rate of 4.8 g/min, and taken up at 500–2000 m/min. The nozzle diameter (D) was 1.0 mm, and L/D = 3. In addition, CO₂ laser irradiation from three directions was focused onto the fibers at a position just under 2.5 mm from the nozzle, and taken up at 500 m/min. This process is hereafter referred to as laser spinning. The random polarized laser beam, whose wavelength and diameter were 10.6 μm and 4.5 mm, respectively, was generated by a PIN-60R laser (Onizuka Glass Co., Ltd.). The emitted laser beam was branched into four by a beam splitter. One branch was used to monitoring the beam power, while the other three were irradiated onto the fiber from three directions at an angle of 120° from each other in a horizontal plane. The laser power per branch was 10 W.

2.2. Drawing

The drawing system was the same as reported elsewhere [11]. A fiber was fed continuously from a feed roller, heated by the CO₂ laser beam, and drawn by the speed difference between the feed and take-up rollers. The fiber running speed after necking was fixed at 110 m/min, and the draw ratio was changed by modulating the fiber feeding speed. A random polarized laser beam with a wavelength and diameter of 10.6 μm and 6 mm, respectively, was generated by a PIN-30R laser (Onizuka Glass Co., Ltd.). The beam was irradiated onto the running fiber from three different directions. The drawing tension was measured by a tension meter (HS-1500S, Eiko Sokki Co., Ltd.). A 100-gf pickup was installed between the neck-drawing point and take-up roller. The drawing stress was calculated from the drawing tension and diameter of the drawn fiber.

2.3. Online measurement

The principle of the online measurement system was reported previously [11]. WAXD/SAXS patterns were obtained by irradiation of an X-ray beam onto the running fiber. The X-ray beam was 40 μm in the vertical direction and 50 μm in the horizontal direction. By moving the laser irradiation position, the distance from the necking point to the X-ray irradiation position was changed. The elapsed time after necking was calculated by dividing the distance by the running speed of the fiber.

The synchrotron X-ray beam used in this study was from SPring-8 BL03XU (FSBL), and an undulator was used to obtain an ultrahigh-intensity X-ray beam. The wavelength of the X-ray beam was 0.10 nm. For WAXD and SAXS measurements, the camera length was 78.7 and 1788 mm, respectively, exposure time for each measurement was 1 and 50 s, respectively, and the detector was a 1032 × 1032 pixel flat panel detector (50 μm/pixel) and 672 × 512 pixel CCD (126 μm/pixel), respectively. After the subtraction of air scattering, the obtained image was normalized by the total

integrated intensity to compensate for the fluctuation of X-ray irradiation volume.

The average position of the necking point and its fluctuation width were determined by analysis of still images taken from the video movie recorded during each measurement. The resolution time was calculated by a reported method [18] by the position resolution, which was calculated from the fluctuation width of the necking point (0.09–0.20 mm), length of the necking point (0.12–0.31 mm), and width of the X-ray beam (0.05 mm). The obtained time resolution was 0.09–0.18 ms.

2.4. Birefringence

The birefringence for each fiber was measured by a polarized microscope (BX51-33POC, Olympus Co., Ltd.) with a monochromic filter of 546 nm. Tricresyl phosphate was used as an immersion oil. The average and standard deviation of birefringence were calculated for 10 samples.

2.5. Thermomechanical tests

Thermal and mechanical properties of drawn fibers were analyzed by tensile tests, thermomechanical analysis (TMA), and differential scanning calorimetry (DSC). The strength, elongation, Young's modulus, and natural draw ratio (NDR) were measured by a universal testing machine (Autograph AGS-X, Shimadzu Co. Ltd.) equipped with a 50-N load cell and air chuck. The sample length and elongation rate were 40 mm and 100 %/min, respectively, and the average and standard deviation of the strength, elongation, and Young's modulus were calculated for every ten samples. The NDR was defined as the draw ratio at which the tensile stress began to rise again with the dissipation of necking point.

A thermomechanical analyzer (TMA/SS6100, SII Nanotechnology Inc.) was used to measure thermal shrinkage factor and shrinkage stress at heating rates of 5 and 10 K/min, respectively. The sample length was 10 mm for both measurements. DSC was conducted using a calorimeter (Thermoplus DSC8230, Rigaku Co. Ltd.) with a heating rate of 10 K/min. A powdered cut fiber sample was used for DSC measurements.

3. Results and discussion

3.1 As-spun fibers

The formation conditions, structure, and physical properties of as-spun fibers are listed in Table 1 and 2. Crystallinity and birefringence increased while NDR and elongation decreased as spinning speed increased. In particular, because of its higher crystallinity and lower cold crystallization temperature than those of the other samples, the fiber taken up at 2000 m/min can be regarded as a POY. In contrast, the laser-spun fiber possesses lower molecular orientation and crystallinity than the fiber spun without laser irradiation. The laser-spun fiber also shows higher NDR and cold crystallization temperature than the others. Both lower spinning speed and laser irradiation of the spin line should decrease the spin line stress, and result in lower molecular orientation of the as-spun fiber. The lower spinning stress should also suppress oriented-induced crystallization, causing the large

NDR and elongation at break.

Table 1 Spinning conditions and structural parameters of as-spun fibers.

Sample	Take-up speed / m/min	Birefringence	NDR	Cold crystallization temperature / °C	Melting temperature / °C	Crystallinity / %
500L	500 (Laser spinning)	0.002	3.4	146	252	5
500	500	0.004	3.0	136	253	8
1000	1000	0.009	2.4	132	254	10
1500	1500	0.019	1.9	126	254	13
2000	2000	0.023	1.5	119	253	26

Table 2 Mechanical and thermomechanical properties of as-spun fibers.

Sample	Tensile strength / MPa	Elongation / %	Young's modulus / GPa
500L	147	620	1.8
500	175	616	2.2
1000	215	407	2.2
1500	283	312	2.3
2000	322	213	2.5

Table 3 Drawing conditions and structural parameters of drawn fibers.

Sample	As-spun fiber	Draw ratio	Laser power /W	Drawing stress /MPa	Fiber temperature /°C		Birefringence	Melting temperature /°C	Crystallinity /%
					0 ms	2 ms			
500L-L	500L	3.4	18.5	16	110	139	0.132	254	27
500L-H		5.1	21	106	146	194	0.213	256	42
500-L	500	3.0	18.4	22	108	136	0.118	255	28
500-H		4.2	21.5	103	142	189	0.182	254	40
1000-L	1000	2.5	22.5	24	104	143	0.129	255	32
1000-H		3.3	23	99	129	178	0.188	257	40
1500-L	1500	2.1	21.1	31	95	134	0.134	256	33
1500-H		2.7	25	105	118	171	0.167	257	38
2000-L	2000	1.9	23.3	48	94	138	0.147	253	34
2000-H		2.1	26.4	109	98	150	0.173	257	38

Table 4 Mechanical and thermomechanical properties of drawn fibers.

Sample	Tensile strength / MPa	Elongation /%	Young's modulus / GPa	Shrinkage at 200 °C / %	Maximum shrinkage stress	
					Stress / MPa	Temperature / °C
500L-L	532	87	6.9	4	18	82
500L-H	1100	29	12.5	9	84	180
500-L	582	95	7.6	5	17	101
500-H	916	38	12.6	9	72	180
1000-L	633	85	8.2	2	27	83
1000-H	897	34	11	8	76	186
1500-L	653	73	7.8	3	26	153
1500-H	847	38	10.8	6	59	195
2000-L	698	52	9.2	4	41	162
2000-H	880	36	11	6	72	194

3.2 Drawing

As shown in previous work, fiber structure development depends on the draw ratio [10]. Therefore, the selection of draw ratio is important to compare the effect of spinning conditions on fiber properties. The minimum and maximum draw ratios that a fiber can be stably drawn at in a continuous drawing process should be strongly related to the NDR and elongation at break of the as-spun fiber, respectively. Therefore, in this study, we planned to select the drawing conditions with both the minimum and maximum stable drawing stress or draw ratio for each set of spinning conditions. Selection of the latter was difficult because the fiber tended to break through the fluctuation of drawing stress during the measurement, so a unified drawing stress of about 100 MPa (actually 99–109 MPa) was used instead of the maximum stable drawing stress. This stress was close to the maximum drawing stress of 109 MPa of a fiber taken up at 2000 m/min, and somewhat lower than that of a fiber taken up at 500 m/min, which can be drawn stably up to a stress of 149 MPa. This indicates that there was a somewhat larger margin of the acceptable draw ratio when the fiber was taken up at 500 m/min; that is, the draw ratio was about 58% of the breaking draw ratio at room temperature, while they were 65%–70% for the other spinning conditions. Meanwhile, the minimum stable draw ratio was almost equal to the NDR except for a take-up speed of 2000 m/min, for which a higher draw ratio was needed to obtain stable drawing.

The drawing conditions, structural parameters, and physical properties of drawn fibers are listed in Table 3 and 4. The minimum stress for stable drawing decreased as spinning speed lowered and also by laser spinning. The minimum drawing stress should correspond to the stress at the natural drawing region, that is, the yield stress. Then, the minimum drawing stress increased with increasing molecular orientation driven by the rise of yield stress. The higher crystallinity, tensile strength, Young's modulus, and shrinkage stress of the minimally drawn fiber can be explained by the increase of drawing stress. In contrast, despite the clear increase of drawing stress, birefringence of the drawn fibers did not change much.

For the fibers exposed to a drawing stress of 100 MPa, the thermal shrinkage, tensile strength, and initial modulus increased with decreasing spinning speed and by laser spinning. Conversely, the elongation at break, thermal shrinkage stress, crystallinity, and birefringence of the fibers did not change much. Although these fibers were drawn under similar drawing stress and possessed similar structural parameters, clear differences in the properties of the drawn fibers were observed for the fibers obtained under different spinning conditions. These results show that the force-bearing structure in the drawn fibers cannot be represented only by crystallinity and birefringence, indicating the necessity of examining additional information about the structure. We explain the dependence of fiber properties on spinning conditions by considering the fiber structure development.

3.3 Fiber temperature profile

Because the crystallization rate depends on temperature, the fiber temperature profiles around the neck drawing point were estimated from the experimental conditions. Profiles were calculated using an energy balance equation that considered laser irradiation energy, heat transfer from the fiber surface, work of plastic deformation by an external force, and latent heat of crystallization [19]. The absorption coefficient of PET of $1.149 \times 10^4 \text{ m}^{-1}$ obtained for the wavelength of the laser beam was used to estimate laser irradiation energy [19]. The heat transfer coefficient was calculated using the experimental formula proposed by Kase and Matsuo [20]. To determine the heat of crystallization, the heat of fusion of drawn fibers was measured by DSC.

The estimated fiber temperature profiles are plotted against the distance from the laser beam axis in Fig. 1. Fiber temperature began to rise from -3 mm when the laser beam begin to irradiate the fibers. When the fiber temperature approached the glass transition temperature of PET, it increased steeply because of the plastic deformation that occurred during necking. The temperature continued to increase after necking because of the laser irradiation and latent heat of crystallization, and reached its maximum value at the edge of the laser beam ($+3 \text{ mm}$). Fiber temperature then decreased to room temperature through heat transfer. Almost the same maximum temperature was estimated for all fibers drawn at the minimum draw ratio (Fig. 1a), while the maximum temperature increased with decreasing spinning speed at a drawing stress of 100 MPa (Fig. 1b). The increase of maximum temperature for the latter situation can be explained by the increase of the applied work for plastic deformation with increasing draw ratio.

As described in Section 3.6, the crystallization rate was estimated from the change of crystallinity until 2 ms after necking in this study. Thus, the estimated fiber temperature immediately after necking and 2 ms after necking are both shown in Table 3 and Fig. 1. The fiber temperature rises about 40 or $50 \text{ }^\circ\text{C}$ in this time for each respective set of drawing conditions.

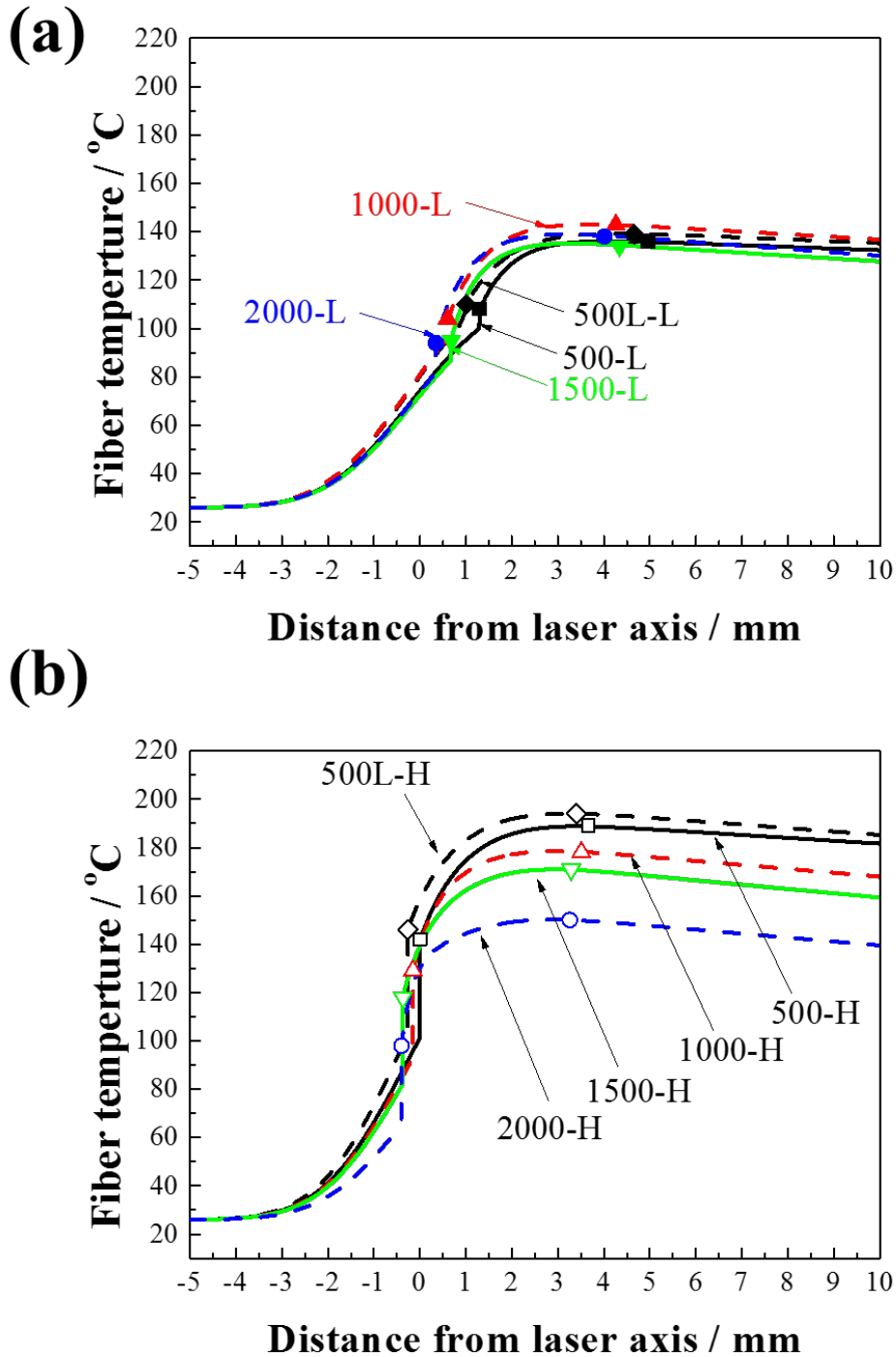


Fig. 1. Estimated fiber temperature profiles plotted against the elapsed time after necking for (a) the minimum draw ratio and (b) a drawing stress of 100 MPa. The estimated fiber temperatures immediately after necking and at 2 ms after necking are shown.

3.4. WAXD patterns

Part of the WAXD images are shown in Fig. 2. Only an amorphous halo was observed for the images obtained with negative elapsed time, that is, before necking. The amorphous halo was concentrated to the equatorial direction immediately after necking, and a streak-like diffraction, assigned to the (001') diffraction of the smectic phase, appeared in the meridional direction after 0.2 ms. With the dissipation of the smectic diffraction, crystal diffractions appeared. The fiber structure development should be almost completed 2.0 ms after necking because the diffraction images are almost the same as those of drawn fibers.

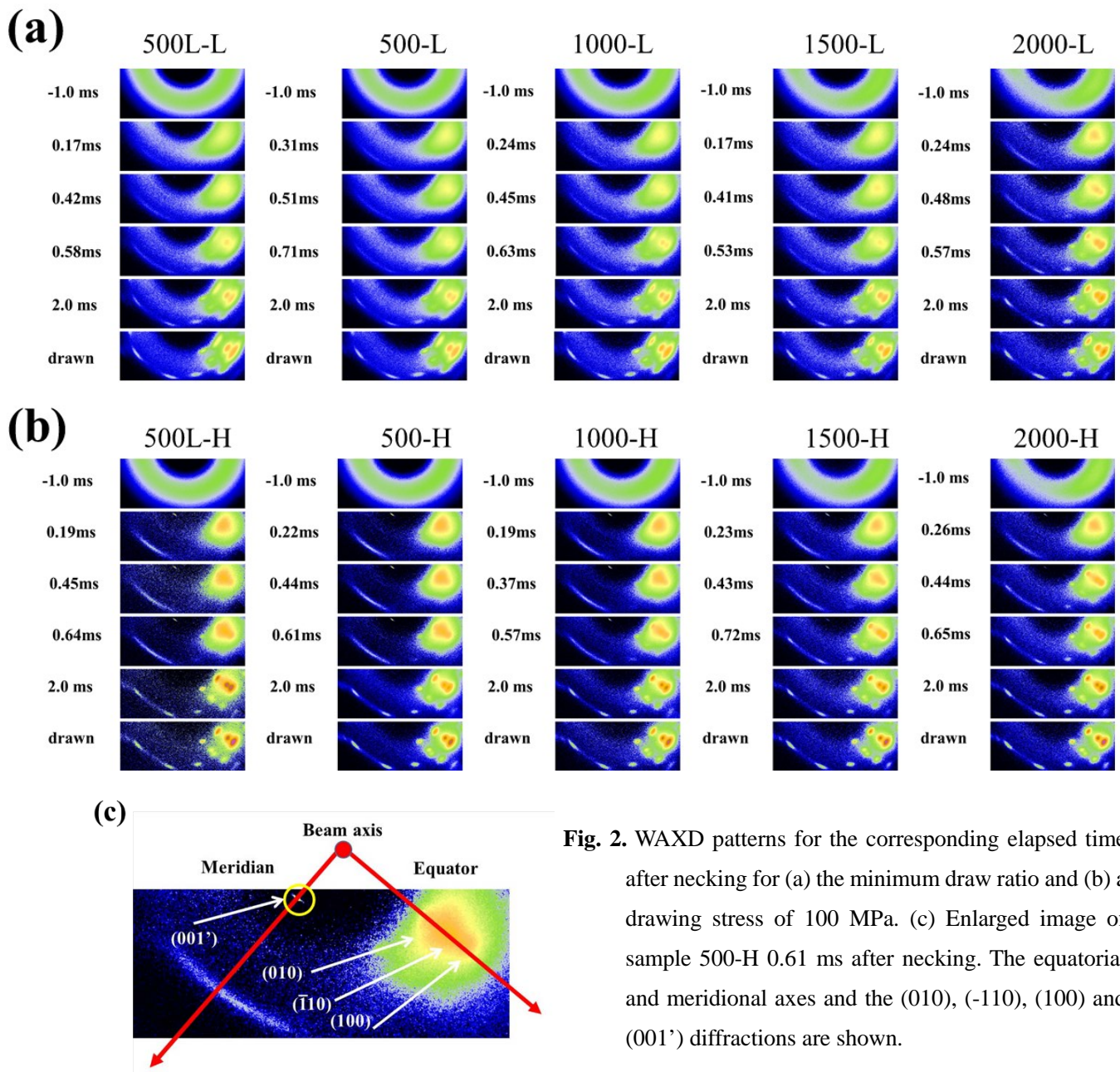


Fig. 2. WAXD patterns for the corresponding elapsed time after necking for (a) the minimum draw ratio and (b) a drawing stress of 100 MPa. (c) Enlarged image of sample 500-H 0.61 ms after necking. The equatorial and meridional axes and the (010), (-110), (100) and (001') diffractions are shown.

3.5. Smectic phase

The smectic phase is a metastable structure first reported by Bonart [21], and has also been observed for PEN [14] and PBT [22]. The smectic phase has been formed during batch drawing [23] and heat treatment of oriented amorphous PET [24]. In this study, a strong (001') diffraction of the smectic phase was observed when the drawing stress was 100 MPa, particularly at low spinning speed. In contrast, a very weak (001') diffraction was observed that disappeared immediately after necking for fibers drawn at the minimum draw ratio. This fact indicates that necking is not sufficient to form the smectic phase at the minimum draw ratio. Instead, an excessive draw ratio over the minimum draw ratio or an excessive drawing stress over the yield stress seems to be necessary to form the smectic phase. This is because the minimum draw ratio is decided by the NDR of the as-spun fiber, and the NDR is closely related to the yield stress. The excessive stress aligns the molecular chains along the fiber axis, and bundles of the aligned molecular chains should form the smectic phase.

Figure 3 and 4 show the meridional integrated intensity and d-spacing of the (001') diffraction of the fibers, respectively. The d-spacing decreased rapidly, and the diffraction almost disappeared within 0.5 ms after necking for the fiber taken up at 2000 m/min. While the intensity of the (001') diffraction clearly increased with lower spinning speed, and was able to be observed for a longer time after necking. In particular, the fibers taken up at 500 m/min showed a clear strong (001') diffraction over 1 ms after necking. Moreover, the laser-spun fiber showed a clear longer time for the decrease of d-spacing. It has been reported that fibers with uniformly distributed entanglements can be obtained by low-speed spinning or laser spinning [2]. Because of the uniform entanglement network in fibers spun at low speed, the drawing stress tends to be applied uniformly to each molecular chain, so more molecular chains are aligned uniformly by the drawing. The uniformly aligned molecular chain should form the highly ordered smectic phase. The smaller applied stress per molecular chain and highly ordered smectic phase can restrict the chain relaxation in the smectic phase, which may cause the longer relaxation time of d-spacing and the longer transition time to the triclinic crystal (see Section 3.6).

The crystallinity and birefringence of drawn fibers were almost the same (Section 3.2). However, the amount of smectic phase and its d-spacing observed immediately after necking showed clear spinning-speed dependence. This is important because the difference in smectic phase can explain the dependence of the properties of drawn fibers on spinning speed. In particular, the tensile and thermomechanical properties of a fiber should be strongly related to the status of the smectic phase because the smectic phase is thought to be bundles of fibrillar molecular chains that bear most of the tensile force in drawn fibers [11]. For example, high-strength drawn fibers can be obtained by taking up fibers at 500 m/min because a large content of the stable smectic phase is formed in the drawing process, which should allow the structure to bear more tensile force. In contrast, the smectic phase should not bear the drawing stress in a fiber taken up at 2000 m/min, in which only a little smectic

phase formed and then vanished immediately. In these PET fibers, the network structure consisting of oriented nuclei formed in the spinning process seems to mainly bear the drawing stress.

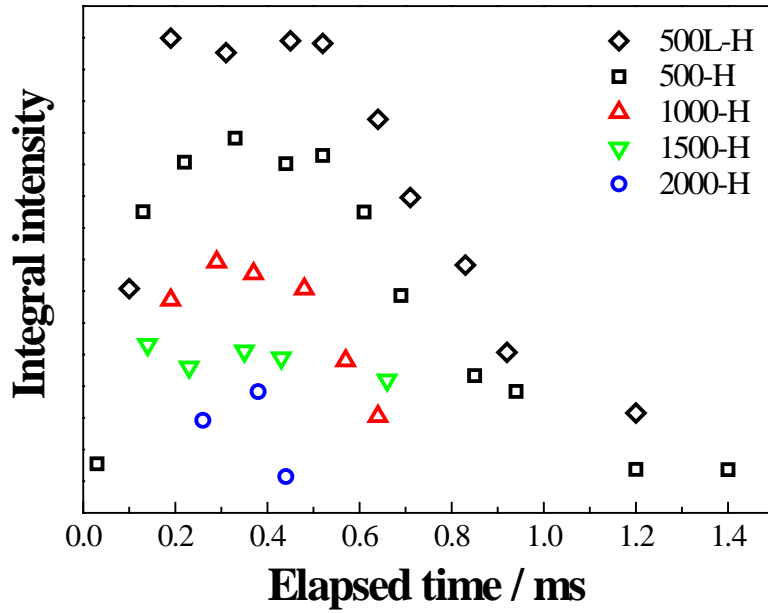


Fig. 3. Integrated intensities of the smectic (001') diffraction plotted against the elapsed time after necking. Sample conditions are shown in figure.

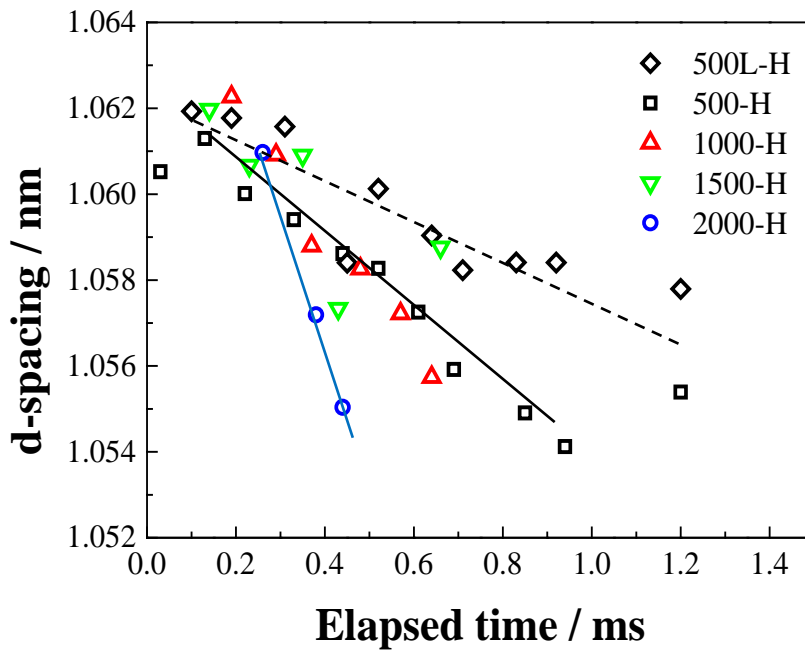


Fig. 4. The d-spacings of the smectic (001') diffraction plotted against the elapsed time after necking. Sample conditions are shown in figure.

3.6. Crystallization rate

The intensity profiles along the equatorial directions were obtained from WAXD patterns of the samples and fitted by Gaussian curves,

$$I(\theta) = I_0 \exp \left\{ -4 \ln 2 \times \left(\frac{2\theta - 2\theta_0}{\beta} \right)^2 \right\}, \quad (1)$$

where 2θ , I_0 , and β are the position, intensity, and full width at half-maximum (FWHM) of the peak, respectively. The equatorial intensity profiles could be separated well into the (010), (-110), and (100) crystal diffractions, and a broad peak consistent with an amorphous or smectic phase. Crystallinity index was determined as the fraction of integrated intensity of the crystal diffractions to the total integrated intensity. Crystallinity indices for all samples started to increase from 0.5 ms after necking, and were almost saturated at 2.0 ms (Fig. 5). Secondary crystallization should occur after that because all the crystallinity indices for drawn fibers were obviously higher than those of respective fibers 2.0 ms after necking. The crystallization rate K_c , crystallization induction time t_0 , and the final crystallinity $X_{c\infty}$ for the fibers were estimated using equation 2 with the crystallinity indices until 2.0 ms after necking, and are presented in Fig. 6.

$$X_{c(t)} = \{1 - K_c \exp(t - t_0)\} X_{c\infty}. \quad (2)$$

Figure 5 reveals that measured crystallinity indices were fitted well with equation 2. For both types of drawing conditions, the crystallization rate decreased with lowering spinning speed and with laser spinning. The crystallization rates for fibers drawn with a drawing stress of 100 MPa were almost the same as those for fibers obtained with the minimum drawing stress except for the fiber taken up at 2000 m/min, for which a larger crystallization rate was observed for drawing under 100 MPa despite it having the smallest difference in drawing stress and draw ratio between them. All crystallization induction times for the minimum draw ratio were about 0.3 ms, and somewhat longer induction times were observed for the fibers spun at lower speed and drawn under 100 MPa.

Fibers spun at low speed displaying almost no dependence of crystallization rate on drawing stress have been reported previously [10]. It was explained that the crystallization acceleration usually observed with molecular orientation was prevented by the delay of crystallization because of the smectic phase formation. This indicates that the crystallites should originate mainly from the smectic phase for the fibers spun at 500-1500 m/min in this study. The clear dependence of crystallization rate on drawing stress observed for the fibers spun at 2000 m/min can be explained by the absence of the

smectic phase at the beginning of crystallization. The crystallization rate increased with increasing molecular orientation because the crystallization was not restricted by the smectic phase, even at a drawing stress of 100 MPa. The oriented nuclei formed in the as-spun fiber should promote crystallite growth during drawing of this fiber, so it showed the highest crystallization rate despite having the lowest fiber temperature.

For PET/polystyrene (PS) conjugated spun fibers, no crystallization induction time was observed after drawing [18]. The authors suggested that the PET component did not bear the drawing stress; instead the PS component mainly bore it. However, the induction time observed for all fibers in this study was no less than 0.3 ms. It is considered that some structure that specifically bears the stress immediately after necking restricted the molecular motion and delayed the beginning of crystallization. For the fiber taken up at 500 m/min and drawn under 100 MPa, this structure should be the smectic phase. A somewhat longer induction time might indicate the higher stability of this phase. Meanwhile, a molecular network including oriented nuclei mainly bore the stress for the fiber taken up at 2000 m/min.

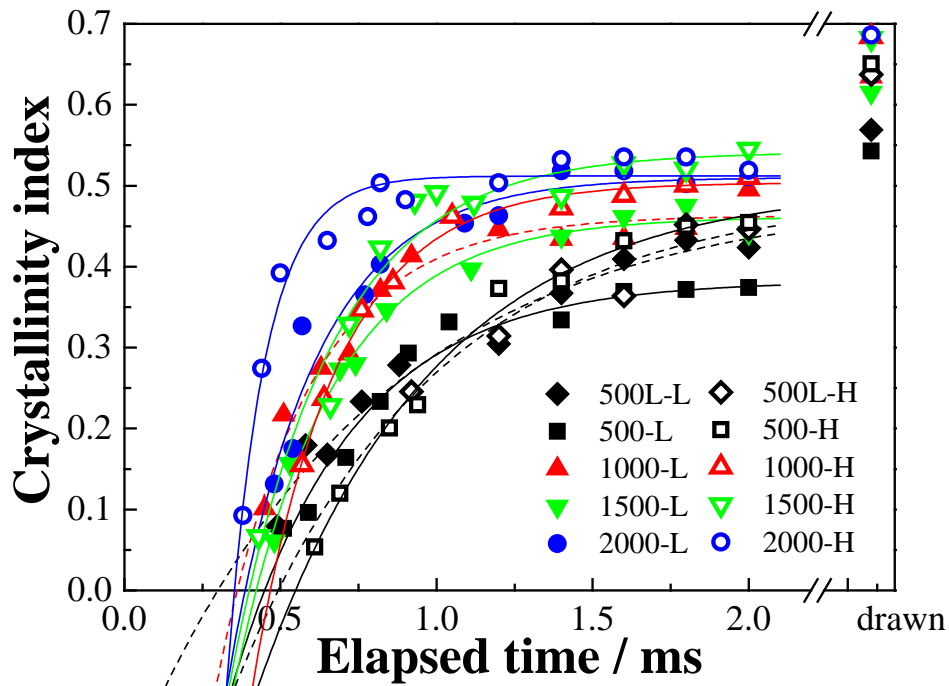


Fig. 5. Crystallinity indices estimated from the WAXD equatorial profiles plotted against the elapsed time after necking. Sample conditions are shown in the figure.

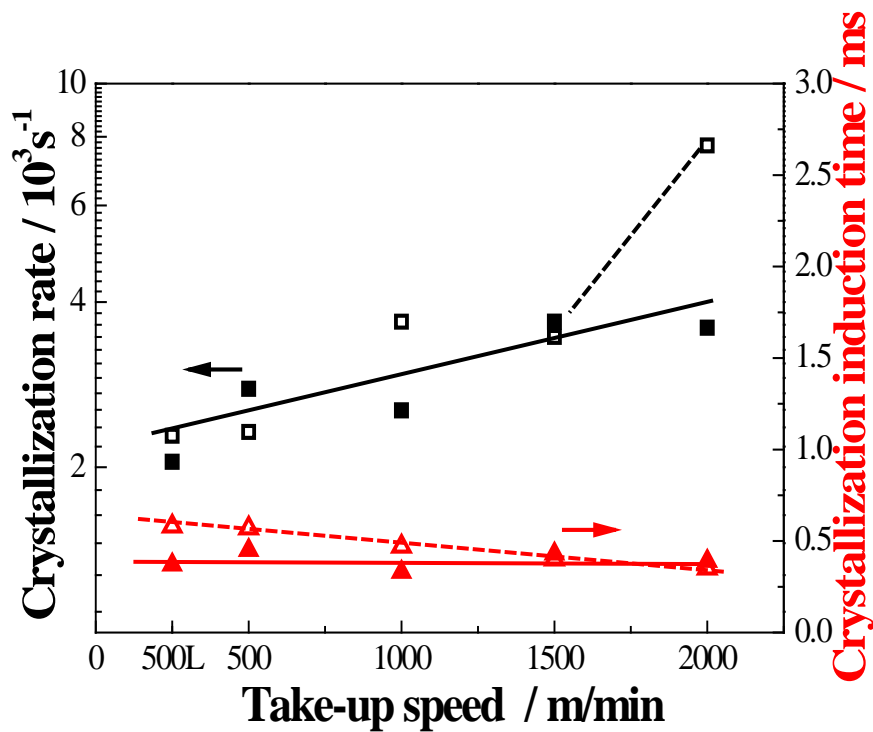


Fig. 6. Crystallization rate and crystallization induction time calculated from the crystallinity indices for fibers drawn with the minimum draw ratio (■ and ▲) and at a drawing stress of 100 MPa (□ and △).

3.7. Crystal orientation

By assuming the orientation axis of each PET crystal was tilted in the (-230) plane from the c -axis [25], the tilting angle and crystal orientation factor were calculated from the intensity profile along the azimuthal angle (φ) . The (010) and (100) diffractions were considered to be two overlapping peaks symmetrical to the equator, and then the intensity profiles can be expressed by equation 3. Each peak was fitted by a Pearson VII type curve, expressed by equation 4, with the peak position (φ_p) and a shape factor m of 2. The measured profiles were fitted well with the curves. The crystal orientation factor (f) , i.e., the orientation factor of the orientation axis to the fiber axis, was obtained by equation 5. The tilting angle (t) was obtained from the peak positions (φ_p) and the d-spacing of (hkl) plane (d_{hkl}) using equation 6. The lattice constants used for the calculation were $a = 0.452$ nm, $b = 0.598$ nm, $c = 1.077$ nm, $\alpha = 101^\circ$, $\beta = 118^\circ$, and $\gamma = 111^\circ$; i.e., those reported by Tomashpol'skii et al. [26].

$$I(\varphi) = i(\varphi, \varphi_p) + i(\varphi, -\varphi_p) \quad (3)$$

$$i(\varphi, \varphi_p) = \frac{I_0}{\left\{ 1 + 4 \left(\frac{\varphi - \varphi_p}{\tau} \right)^2 \left(2^{\frac{1}{m}} - 1 \right) \right\}^m} \quad (4)$$

$$f = \frac{3 \langle \cos^2 \varphi \rangle - 1}{2}, \quad \langle \cos^2 \varphi \rangle = \frac{\int_0^{\pi/2} i(\varphi, 0) \cos^2 \varphi \sin \varphi d\varphi}{\int_0^{\pi/2} i(\varphi, 0) \sin \varphi d\varphi} \quad (5)$$

$$\cos \varphi_p = d_{hkl} \left[\left(\frac{h}{2} + \frac{k}{3} \right) c \sqrt{\frac{1 - \cos^2 t}{c^2 L - K^2}} + \frac{l}{c} \left(\cos t - K \sqrt{\frac{1 - \cos^2 t}{c^2 L - K^2}} \right) \right] \quad (6)$$

$$\text{Where, } K = \frac{ac}{2} \cos \beta + \frac{bc}{3} \cos \alpha, \quad L = \frac{a^2}{4} + \frac{b^2}{9} + \frac{ab}{3} \cos \gamma$$

The obtained f and t are shown in Fig. 7. There were almost no changes in f and t observed for all samples after the crystal diffraction was clearly detected. With increasing spinning speed for the minimum draw ratio, t decreased while f of the (010) plane increased. These tendencies can be explained by the increase of drawing stress. However, a small t and large f of the (100) plane were also observed for the laser-spun fiber despite it having the lowest drawing stress of the samples. The reason for this is not clear. In contrast, both f and t became saturated for fibers drawn at a drawing stress of 100 MPa at f of over 0.98 and t of less than 3° .

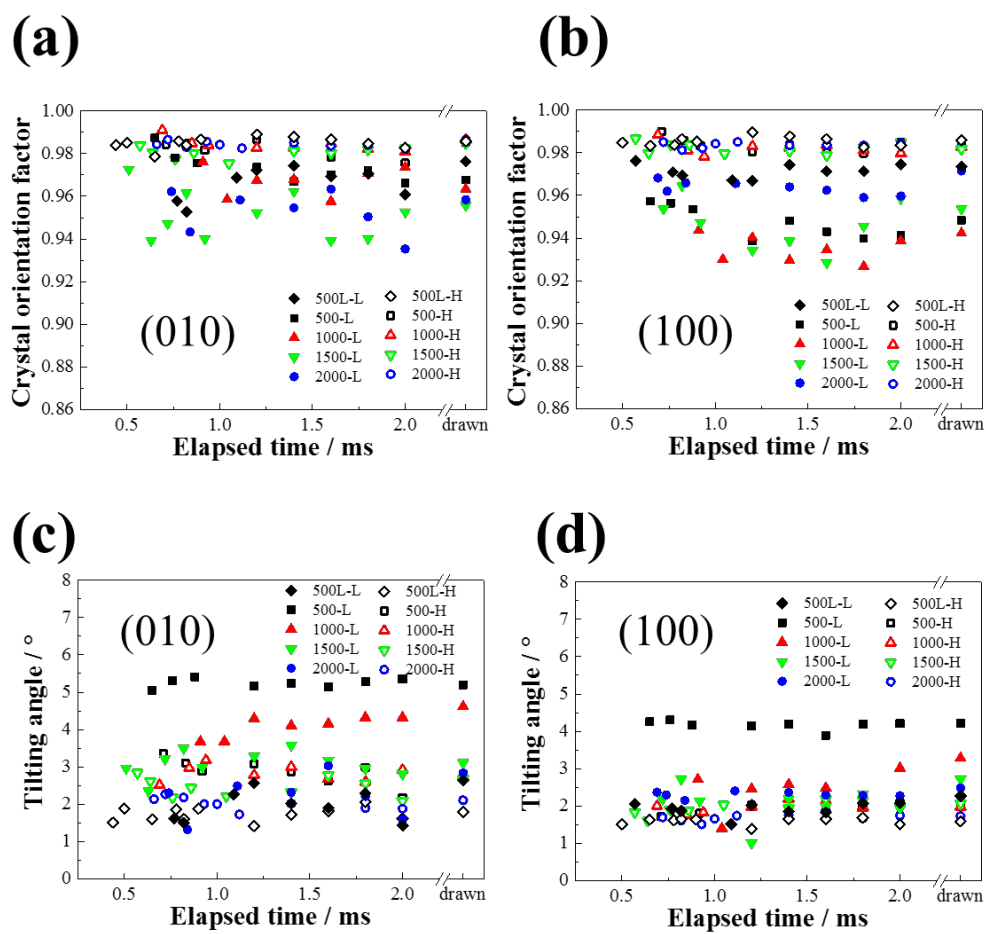


Fig. 7. (a, b) Crystal orientation factors and (c, d) tilting angles of the (010) and (100) planes of the fibers. Sample conditions are shown in the figure.

3.8. SAXS patterns

Part of the SAXS images are shown in Fig. 8. By drawing at the minimum draw ratio, an X-shaped pattern appeared about 0.3 ms after necking, and then changed to a four-point pattern for all spinning conditions (Fig. 8a). On the contrary, for a drawing stress of 100 MPa, although the patterns finally became a similar equatorial bar-like pattern, clear spinning condition dependence was observed in the initial stage of structure development (Fig. 8b). That is, the four-point pattern similar to that found with minimum drawing stress was observed at about 0.3 ms, and it changed to the bar-like pattern, probably because of the overlap of the meridional two-point patterns, as time elapsed for the fiber taken up at 2000 m/min. While a bar-like pattern was already observed at 0.4 ms, it shifted gradually to higher angle for the fibers taken up at 500m/min.

An X pattern was also reported for fibers drawn with the minimum draw ratio, and was explained by the shear-band-like structure formed by necking [10, 27]. The shear-band-like structure should be a molecular bundle aligned along the shear plane. The four-point SAXS pattern can also be explained by the crystallites formed along the shear plane. Incidentally, it has been proposed that an entangled molecular network forms in the as-spun fibers [28]. Therefore, at necking for the minimum draw ratio, the shear deformation is thought to be terminated by the extension of part of the molecular network. Despite the clear dependence of the spinning conditions on drawing stress, the similar structure development for the minimum draw ratio indicates that the molecular bundle aligned along the shear plane does not directly bear the drawing stress and tensile force applied to the drawn fiber. Therefore, there must be force-bearing chains connecting the entanglements in molecular bundles. These force-bearing chains are thought to be a part of the molecular network mentioned above, and the crystallites seemed to be developed from the force-bearing chains. Crystallites surrounded by the molecular bundle involving entanglements was also supposed for nano-oriented crystals [29].

A four-point pattern was observed in the initial stage of structure development for the fibers taken up at 2000 m/min even under a drawing stress of 100 MPa. This indicates that crystallites also formed along the molecular bundle aligned along the shear plane in this case. Thereafter, the gradual pattern change suggests the rearrangement of crystallites along the oriented nuclei formed in the spinning process, which is probably caused by relaxation of the molecular bundle. The crystallites grown from the oriented nuclei seemed to bear most of the drawing stress, whereas the crystallites formed along the shear plane hardly bore any stress. By interlocking the crystallites with large internal differences in borne stress, the thermal shrinkage of obtained fibers is thought to be restricted because the crystallites originally formed along the shear bands block the thermal shrinkage.

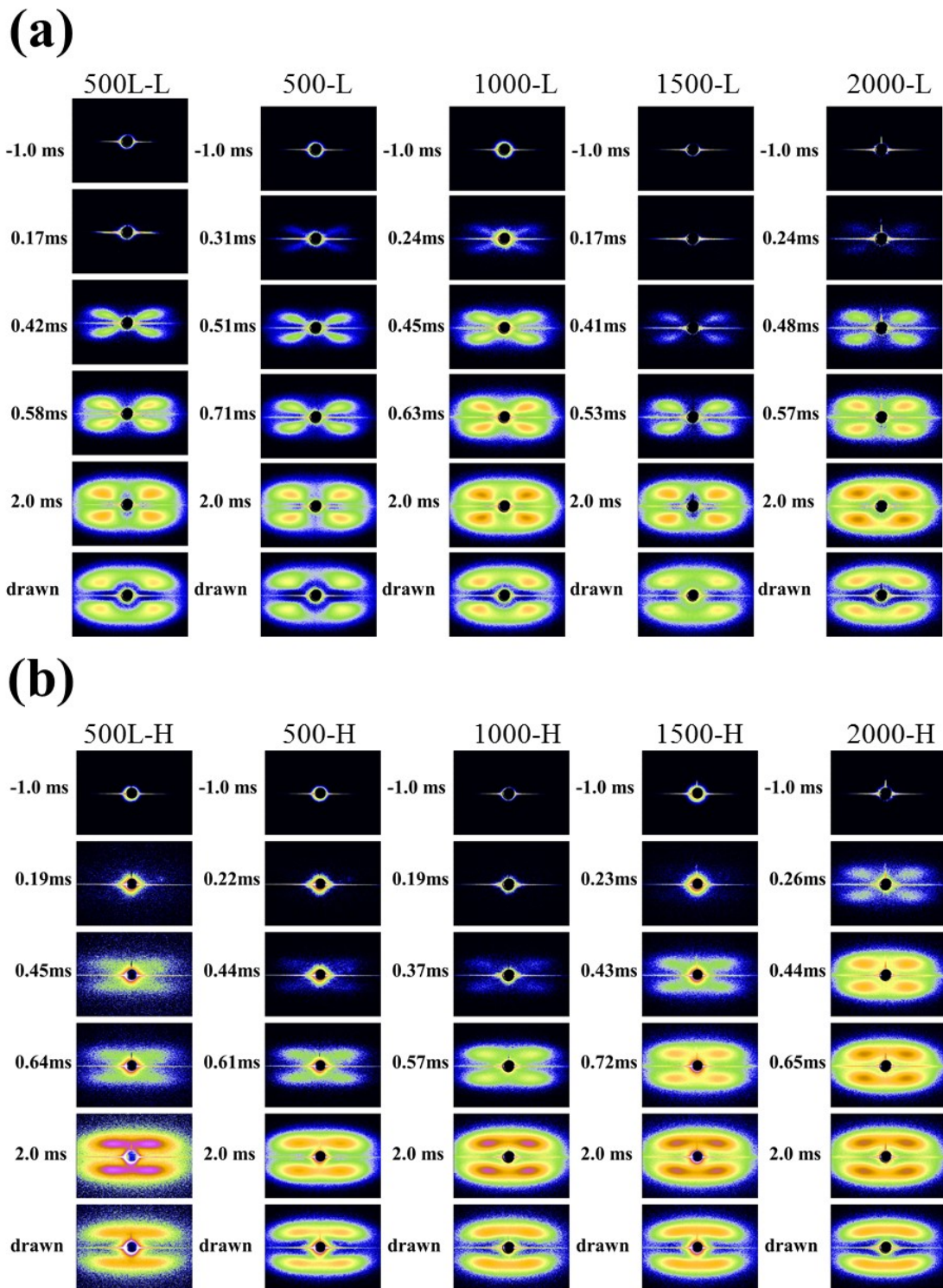


Fig. 8. SAXS patterns at different elapsed times for fibers after necking drawn at (a) the minimum draw ratio and (b) a drawing stress of 100 MPa.

3.9. Long period

The long period shown in Fig. 9 was calculated by the Bragg formula from the peak position obtained by fitting each meridional SAXS profile with a Gaussian curve and base line. The long period increased with drawing stress. In particular, the larger long period in the initial stage of structure development and a steep decrease until 2.0 ms were observed for the fibers spun at 500 m/min and then drawn under a stress of 100 MPa. In contrast, most crystallites should be formed together with the periodic structure for the other samples because the long period did not change much.

The decrease in the long period and the low crystallization rate observed for the fibers spun at 500 m/min and drawn under a stress of 100 MPa suggest that the crystallites formed gradually from the smectic phase. Yamaguchi et al [11] also observed these phenomena and proposed a model in which the fibrillar smectic phase was transformed into a microfibril structure consisting of a sequence of crystallites and amorphous phases connected by tie chains. Because the smectic phase is thought to be formed mainly by extended polymer chains, numerous taut tie chains bearing the external force should be formed in the amorphous phase. Moreover, the development of bar-like patterns without passing through the four-point pattern indicates that the microfibril developed directly from the aligned molecular bundle formed at necking by way of fibrillar-shaped smectic phase. Therefore, a tightly interlocked structure hardly formed between the fibrils. As a result, fibers possessing high strength but also large thermal shrinkage tend to be formed by the high-ratio drawing of fibers spun at low speed.

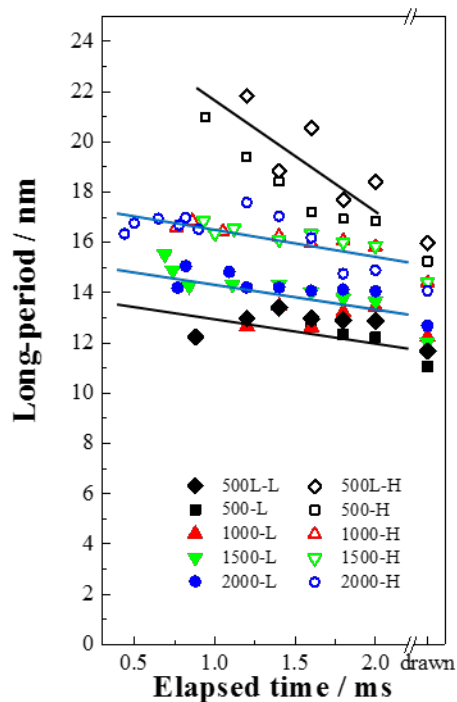


Fig. 9. Long periods obtained from SAXS patterns plotted against the elapsed time after necking. Sample conditions are shown in figure.

3.10. Effect of spinning conditions on fiber structure development

Schematic diagrams of fiber structure development are shown in Fig. 10. By drawing at the minimum stable draw ratio, crystallites appear to be formed along the shear-band-like structure formed by necking. The NDR is influenced by the structural organization [30]. Because the shear deformation caused by necking changes the entangled chain network to a shear-band-like structure with connective chains, the size and orientation of the entangled molecular network formed in the melt-spinning process [2] determines the NDR. Although the X-shaped SAXS pattern was observed for all spinning conditions, the drawing stress increased with the spinning speed. The increase of drawing stress increases the molecular orientation, which raises the crystallization rate and changes the properties of the drawn fiber.

Clear dependence of the structure development on spinning speed was observed for the high-ratio drawing under high drawing stress. The smectic phase should preferentially form in fibers spun at low speed or by laser spinning, while the oriented nuclei formed in the spinning process tend to grow in fibers spun at high speed. By drawing fibers spun at low speed over their NDR, the smectic phase is considered to be oriented chain bundle formed by the excessive drawing of the shear-band-like structure. Because the maximum draw ratio is decided by the entanglement structure in the as-spun fibers, the length and amount of smectic phase should depend on the spinning conditions. Therefore, structure development is typically observed for fibers spun at 500 m/min with a uniform entangled molecular network [2]. Take-up speeds of no more than 1500 m/min are thought to be included in this category of structure development in this study. The maximum draw ratio and amount of smectic phase decreased with increasing spinning speed. Drawing at high strain rate in a high-speed spin line produced a molecular network with nonuniform entanglement density, which caused stress concentration at specific areas, inducing solidification of the fiber through the formation of oriented nuclei in the force-bearing chain. The stress should also be concentrated on the molecular network in the drawing process, and then the crystallites formed by the oriented nuclei seem to grow preferentially in this case. However, the above-mentioned shear-band-like structure was also formed in the fibers taken up at 2000 m/min because they showed clear necking and a four-point SAXS pattern during the initial stage of structure development. The mixture of these two mechanisms might be typical structure development of a POY. The fiber spun at the higher speed, a so-called fully oriented yarn, should be another extreme model of the fiber structure development. Because orientation-induced crystallization proceeded on the spin line, the as-spun fiber was mainly composed of the crystallites formed in the spin line [31]. Stable neck drawing is no longer possible in this case because of the dissipation of the natural drawing region.

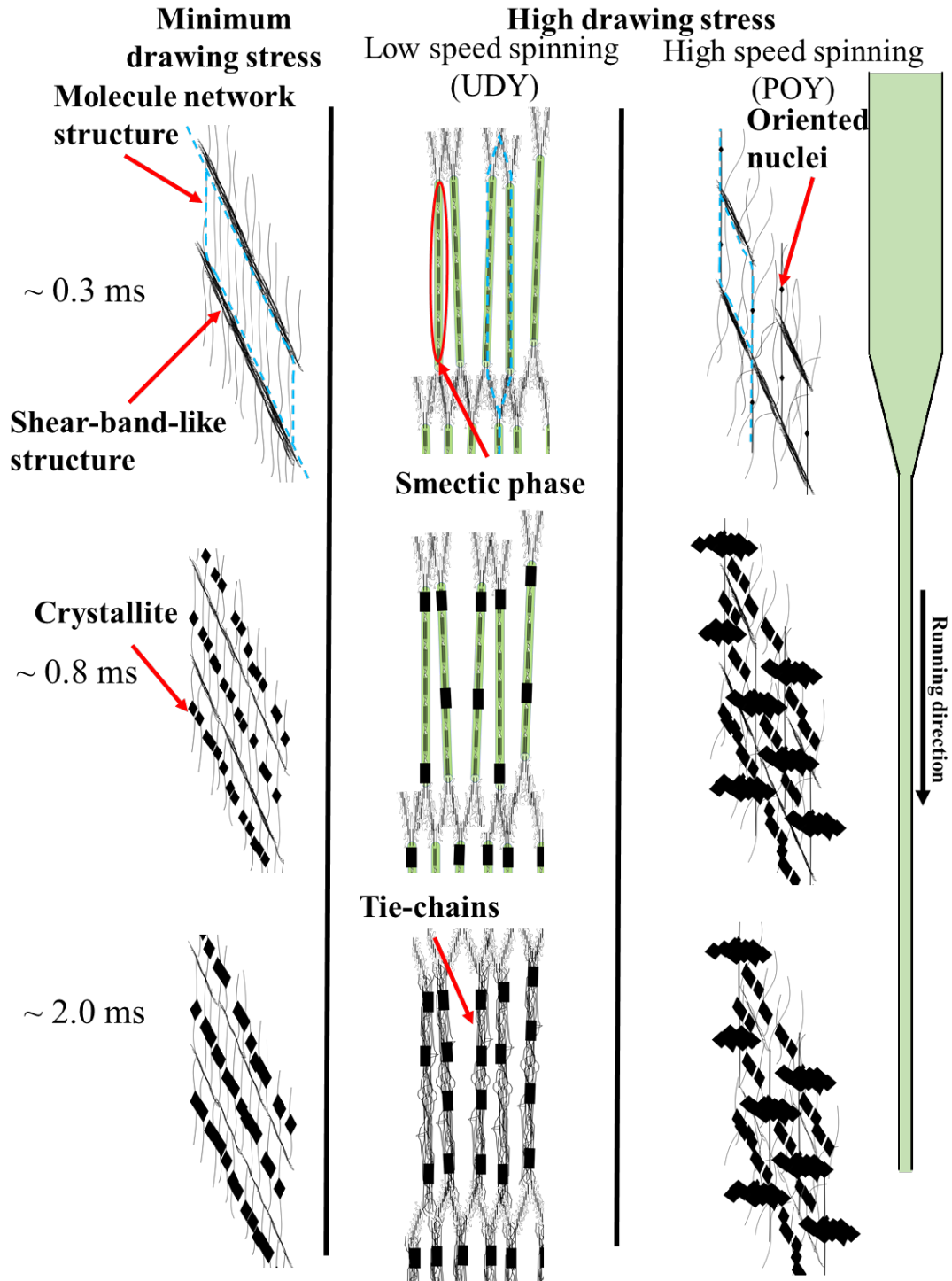


Fig. 10. Schematic diagram of fiber structure development. The structures of the molecular network in the fibers are shown as blue lines.

4. Conclusions

The effects of spinning conditions on the structure development of PET fibers after necking were analyzed by WAXD/SAXS measurements. Fibers obtained with a spinning speed of 500–2000 m/min were used for the measurements. The fibers obtained from laser spinning using a CO₂ laser beam irradiated onto the fiber at the melt spinning line were also analyzed. The as-spun fibers were drawn continuously at the minimum stable draw ratio and under a drawing stress of about 100 MPa. The latter was almost the maximum drawing stress at which all the as-spun fibers could be drawn stably. The WAXD and SAXS images were captured simultaneously until 2.0 ms after necking using synchrotron radiation. The time resolution of the measurements was 0.09–0.18 ms.

An X-shaped SAXS pattern was observed about 0.3 ms after necking for all fibers drawn at the minimum stable draw ratio. This indicates that necking, which determines the minimum stable draw ratio, decided the fiber structure development.

In contrast, clear dependence of the structure development on spinning speed was observed for fibers drawn under a drawing stress of 100 MPa. A strong smectic (001') diffraction and larger long period, particularly less than 1 ms after necking, were observed for the fibers spun at 500–1500 m/min, while almost no smectic phase was observed at the beginning of crystallization for that spun at 2000 m/min. A higher crystallization rate and clear draw ratio dependence of crystallization rate were also observed for the fiber spun at 2000 m/min despite it having the lowest fiber temperature and smallest difference in drawing stress of the fibers investigated.

These results suggest the crystallites were mainly formed by the phase separation of the fibrillar smectic phase for the fibers spun at 500–1500 m/min, while they mainly developed from the oriented nuclei formed in the spinning process for the fibers spun at 2000 m/min. Although no marked differences of birefringence, crystallinity, and SAXS patterns were observed for the drawn fibers, there were clear differences in their tensile strength and thermal shrinkage behavior. The clear differences in structure development described above indicate the capability of structure development analysis to aid in designing fiber properties.

Acknowledgments

This study was supported by Grants-in-Aid for Scientific Research (No. 23550240 and 16K05910) from the Ministry of Education and Science Ministry, Japan. Experiments were performed at the SPring-8 synchrotron radiation facility (No. 2013B7263).

References

- 1) Y. Liu, L. Yin, H. Zhao, G. Song, F. Tang, L. Wang, H. Shao, Y. Zhang, *J. Appl. Polym. Sci.*, 2015, DOI: 10.1002/APP. 42512.
- 2) M. Masuda, Y. Funatsu, K. Kazama, T. Kikutani, *Sen'i Gakkaishi*, 60, (2004), 338-345.
- 3) M. Masuda, W. Takarada, T. Kikutani, *Int. Polym. Process*, 25, (2010), 159-169.
- 4) T. Kikutani, J. Radhakrishnan, S. Arikawa, A. Takaku, N. Okui, X. Jin, F. Niwa, Y. Kudo, *J. Appl. Polym. Sci.*, 62, (1996), 1913-1924.
- 5) J. Radhakrishnan, T. Kikutani, N. Okui, *Text. Res. J.*, 67, (1997), 684-694.
- 6) H. J. Jeon, H. Ito, T. Kikutani, N. Okui, M. Okamoto, *J. Appl. Polym. Sci.*, 70, (1998), 665-674.
- 7) W. Takarada, H. Ito, T. Kikutani, N. Okui, *J. Appl. Polym. Sci.*, 80, (2001), 1575-1581.
- 8) K. Nakata, Y. Ohkoshi, Y. Gotoh, M. Nagura, Y. Funatsu, T. Kikutani, *Sen'i Gakkaishi*, 60, (2004), 352-355.
- 9) K. Nakata, F. Nakamura, Y. Ohkoshi, Y. Gotoh, M. Nagura, A. Hamano, S. Takada, T. Kikutani, *Int. Polym. Process*, 27, (2012), 386-391.
- 10) R. Tomisawa, T. Ikaga, K. H. Kim, Y. Ohkoshi, K. Okada, H. Masunaga, T. Kanaya, M. Masuda, Y. Maeda, *Polymer*, Submitted(JPOL-S-16-02834)
- 11) T. Yamaguchi, K. H. Kim, T. Murata, M. Koide, S. Hitoosa, H. Urakawa, Y. Ohkoshi, Y. Gotoh, M. Nagura, M. Kotera, K. Kajiwara, *J. Polym. Sci., Polym. Phys.*, 46, (2008), 2126-2142.
- 12) K. H. Kim, T. Yamaguchi, Y. Ohkoshi, Y. Gotoh, M. Nagura, H. Urakawa, M. Kotera, T. Kikutani, *J. Polym. Sci., Polym. Phys.*, 47, (2009), 1653-1665.
- 13) K. H. Kim, T. Murata, Y. A. Kang, Y. Ohkoshi, Y. Gotoh, M. Nagura, H. Urakawa, *Macromolecules*, 44, (2011), 7378-7384.
- 14) K. H. Kim, R. Aida, Y. A. Kang, T. Ikaga, Y. Ohkoshi, I. Wataoka, H. Urakawa, *Polymer*, 53, (2012), 4272-4279.
- 15) Y. A. Kang, K. H. Kim, S. Ikehata, Y. Ohkoshi, Y. Gotoh, M. Nagura, M. Koide, H. Urakawa, *Polymer*, 52, (2011), 2044-2050.
- 16) K. Ide, T. Ikaga, Y. Ohkoshi, I. Wataoka, M. Masuda, Y. Maeda, *Sen'i Gakkaishi*, 70, (2014), 76-83.
- 17) K. H. Kim, Y.A. Kang, A. Yokoyama, T. Ikaga, Y. Ohkoshi, I. Wataoka, H. Urakawa, *Polymer*, 44, (2012), 1030-1035.
- 18) K. Sugawara, T. Ikaga, K.H. Kim, Y. Ohkoshi, K. Okada, H. Masunaga, T. Kanaya, M. Masuda, Y. Maeda, *Polymer*, 79, (2015), 37-46.
- 19) W. Okumura, T. Yamaguchi, Y. Ohkoshi, Y. Gotoh, M. Nagura, *Intern. Polym. Proc.*, 17, (2002), 124-132.
- 20) S.Kase, and T.Matsuo, *Journal of Polymer Science Part A: General Papers*, 3, 2541, (1965)
- 21) R. Bonart, *Kolloid-Z*, 213, (1966), 1-11.

- 22) T. Konishi, Y. Miyamoto, *Polymer*, 42, (2010), 349-353.
- 23) D. Kawakami, B. S. Hsiao, C. Burger, S. Ran, C. Avila-Orta, I. Sics, T. Kikutani, B. Chu, *Macromolecules*, 38, (2005), 91-103.
- 24) T. Asano, F. J. Balta Calleja, A. Flores, M. Tanigaki, M. Mina, C. Sawatari, H. Itagaki, H. Takahashi, I. Hatta, *Polymer*, 40, (1999), 6475-6484.
- 25) R. P. Daubeny, C. W. Bunn, *J. Polym. Sci., Polym. Chem.* 226, (1954), A1954, 531.
- 26) Y. Y. Tomashpol'skii, G. S. Markova, *Polym. Sci. USSR*, 6, (1964), 316-324.
- 27) K. Okada, M. Nakada, Y. Higashioji, K. Takahashi, Y. Ohkoshi, T. Kanaya, *Koubunshi Ronbunshu*, 71, (2014), 593-600.
- 28) T. Kikutani et al. "Fundamental and Practical Technologies for Nano-structured Polymeric Materials", 2008, p.56-110, CMC press, ISBN978-4-7813-0043-6.
- 29) K. N. Okada, J. Washiyama, K. Watanabe, S. Sasaki, H. Masunaga, M. Hikosaka, *Polymer*, 42, (2010), 464-473.
- 30) M. Kuriyagawa, K. Nitta, *Polymer*, 52, (2011), 3469-3477.
- 31) J. Shimizu, T. Kikutani, A. Takaku, N. Okui, *Sen'i Gakkaishi*, 40, (1984), T177-183.